# State Transition Modeling Method for Optimal Dispatching for Integrated Energy System Based on Cyber–Physical System

Yi Yang, Peng Zhang, Can Wang, Zhuoli Zhao, and Loi Lei Lai

***Abstract*—The traditional energy hub based model has difficulties in clearly describing the state transition and transition conditions of the energy unit in the integrated energy system (IES). Therefore, this study proposes a state transition modeling method for an IES based on a cyber-physical system (CPS) to optimize the state transition of energy unit in the IES. This method uses the physical, integration, and optimization layers as a three-layer modeling framework. The physical layer is used to describe the physical models of energy units in the IES. In the integration layer, the information flow is integrated into the physical model of energy unit in the IES to establish the state transition model, and the transition conditions between different states of the energy unit are given. The optimization layer aims to minimize the operating cost of the IES and enables the operating state of energy units to be transferred to the target state. Numerical simulations show that, compared with the traditional modeling method, the state transition modeling method based on CPS achieves the observability of the operating state of the energy unit and its state transition in the dispatching cycle, which obtains an optimal state of the energy unit and further reduces the system operating costs.**

***Index Terms*—Integrated energy system (IES), cyber-physical system (CPS), state transition, modeling, optimal dispatching.**

## I. Introduction

BUILDING a new power system dominated by renewable energy sources (RESs) is critical for achieving carbon peaking and carbon neutrality. An integrated energy system (IES) integrates various energy sources such as cooling, heating, electricity, and gas. As a major utilization form of RESs, IES is a representative of new power system [1], [2]. To fully utilize the economy and flexibility of an IES, a reasonable and effective dispatching strategy is required to coordinate the operation of multiple energy units [3]. Modeling, as the basis of the optimal dispatching of an IES, significantly affects the economy of the optimal dispatching of IES [4]. Therefore, the reasonable and accurate modeling is of great significance.

Studies have been conducted on the modeling of IES, including modeling from a single energy unit to the system level. For example, [5] provides the detailed modeling of a single energy unit in an IES. Reference [6] divides the IES into electric power, thermal, and cold subsystems based on the energy bus architecture and then models them separately. At the system level, [7] proposes a general system modeling method based on unified energy flow to describe the static relationship of system energy flow. Reference [8] provides a unified modeling method for electric power, natural gas, and thermal subsystems based on the energy circuit, which is widely used in large-scale energy transmission networks. For the small-scale IES, the energy hub (EH) based model proposed by the Swiss Federal Institute of Technology has been acknowledged by many researchers [9], [10]. The EH-based model describes the relationship among energy transmission, conversion, distribution, and storage in an IES through efficiency and distribution coefficients, and is widely used in many areas such as the planning of IESs [11], the management of distributed energy system [12], and the dispatching of regional energy system [13]. However, the EH-based model only reflects the static relationship of energy in transmission and conversion links, and the description of a single energy unit remains insufficient.

In short, some preliminary results have been achieved in the IES modeling, but there are still some limitations that need to be addressed.

1) There are a large number of energy units in the IES, and their states vary during operation. The starting, operating, and stopping states constitute a set of different operating states for energy units in the IES. It is challenging to use a unified model to characterize the multiple operating states and the transitions between the states to improve the observability of IES.

2) The economy of the dispatching of IES depends on the accuracy of the IES model. However, the existing studies tend to simplify the IES model to a certain extent and lack an accurate description of the operating state of each energy

Manuscript received: January 23, 2024; revised: March 11, 2024; accepted: April 19, 2024. Date of CrossCheck: April 19, 2024. Date of online publication: May 29, 2024.

This work was supported by the National Natural Science Foundation of China (No. 52107108).



Y. Yang (corresponding author), P. Zhang, and C. Wang are with the Hubei Provincial Key Laboratory for Operation and Control of Cascaded Hydropower Station, College of Electrical Engineering and New Energy, China Three Gorges University, Yichang, China (e-mail: epyyang@163.com; yyhandsome018@126.com; xfcancan@163.com).

Z. Zhao and L. L. Lai are with the Department of Electrical Engineering, School of Automation, Guangdong University of Technology, Guangzhou, China (e-mail: zhuoli.zhao@gdut.edu.cn; l.l.lai@ieee.org)

DOI: 10.35833/MPCE.2024.000090

unit. Thus, they fail to reflect the changes in the operating states of energy units and the energy conversion process of the energy unit under different states, which affect the accuracy of the dispatching scheme of IES.

3) The aforementioned studies only model the physical system of an IES from the internal coupling characteristics of energy flow, ignoring the effects of information flow during IES operation. To fully reveal the interplay of the information flow and energy flow in the IES, and to visualize the operating state and state transition of energy unit in the IES, the cyber and physical systems should be studied as an integrated system for modeling analysis.

To address these issues, researchers have begun to seek new modeling methods, among which the modeling based on cyber-physical systems (CPSs) has received wide attention. The theory of CPS provides a technical means for realizing the integrated modeling of physical and cyber systems in an IES. A CPS, through a closed-loop mechanism of sensing, analysis, decision-making, and execution, can detect the operating state of an energy unit in an IES in real time, and thus realize the observability and controllability of IES. The power grid CPS has been widely studied in recent years [14]. For example, [15] proposes an equivalent cyber-physical model for power grids to evaluate the effects of cyber-side contingencies on the physical system. In [16] and [17], a general model of a time-delayed CPS under fully distributed control is proposed to analyze the effects of time delay on the stability of a power grid CPS, combining the dynamics of the physical system. Reference [18] proposes a robust routing model for CPS with a priority mechanism while considering cyber-physical disturbances to improve the robustness of smart grids in dealing with possible cyber-physical coupling failures. Reference [19] proposes a CPS model that reflects the correlation between information and energy flows, which effectively improves the power supply reliability of the system under extreme cyberattack scenarios. Reference [20] proposes a CPS resilience assessment model that considers the space time of disasters and the interaction between information systems and the power grid, which effectively improves the ability to withstand typhoons. Reference [21] proposes a power grid CPS model considering cyber congestions for analyzing information flow of cyber systems and cyber contingencies. Reference [22] considers multi-dimensional uncertainties in both cyber and physical spaces and proposes a planning model of power grid CPS based on two-layer optimization for optimizing the location and selection of active-management elements.

Existing power grid CPS models have achieved the integrated modeling of cyber and physical systems; however, they fail to realize the description of the state transition of energy unit. The integration of information flow into the physical model of energy units in the IES and the construction of the state transition model of IES based on CPS are the key issues addressed in this study.

Thus, this study proposes a state transition model for an IES based on CPS and applies it to the day-ahead optimal dispatching of IES. The main contributions of this study are summarized as follows.

1) A CPS-based hierarchical modeling framework for an IES is proposed, and different methods are utilized to model each layer. The hierarchical modeling framework integrates energy and information flows and can be extended to other energy systems with the integration of CPS.

2) A method for the division of operating states of energy units based on the load ratio is proposed. The refined division can delineate the operating characteristics of energy units more precisely, which makes the dispatching scheme of IES more reasonable and reduces the operating costs of IES.

3) The information flow is integrated into the physical model of energy unit in IES, and the state transition model of energy unit based on the CPS is established, which can visualize the operating state and state transition of energy unit.

The remainder of this paper is organized as follows. Section II describes the architecture of IES based on CPS and hierarchical modeling framework. Section III discusses the state transition model of the IES based on CPS. Case studies are presented in Section IV. Section V concludes this study.

## II. Architecture of IES Based on CPS and Hierarchical Modeling Framework

### A. Architecture of IES Based on CPS

The architecture of IES based on CPS studied in this paper is shown in Fig. 1, which consists of two parts: the physical system and the cyber system.

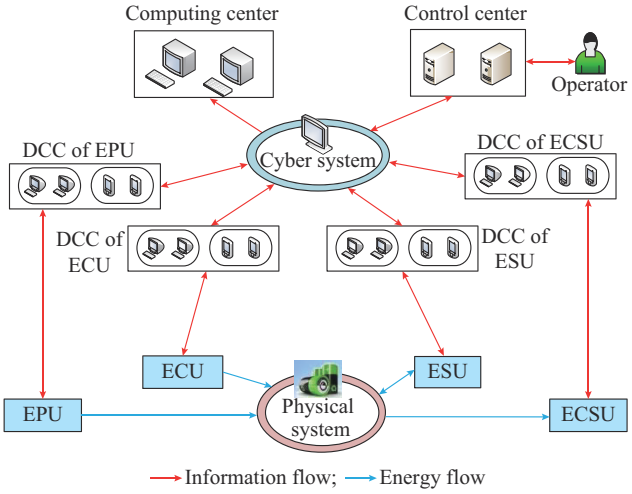


Fig. 1. Architecture of IES based on CPS.

The physical system consists of energy production units (EPUs), energy conversion units (ECUs), energy storage units (ESUs), and energy consumption units (ECSUs), which are used in the production, conversion, storage, and consumption of different energy sources, respectively.

The cyber system consists of data collection and control (DCC) of energy units, computing center, control center, and a communication network that connects these cyber devices. As the control center of IES, the cyber system is responsible for data monitoring and optimization decisions of IES as well as the analysis of information uploaded from the physi-

cal system and for the generation of the corresponding control commands for issuance.

### *B. Hierarchical Modeling Framework*

To fully reveal the interplay between the information and energy flows in an IES and to visualize the operating state and state transition of each energy unit in the IES, we propose a hierarchical modeling framework for an IES integrated with a CPS, as shown in Fig. 2, which consists of physical, integration, and optimization layers.

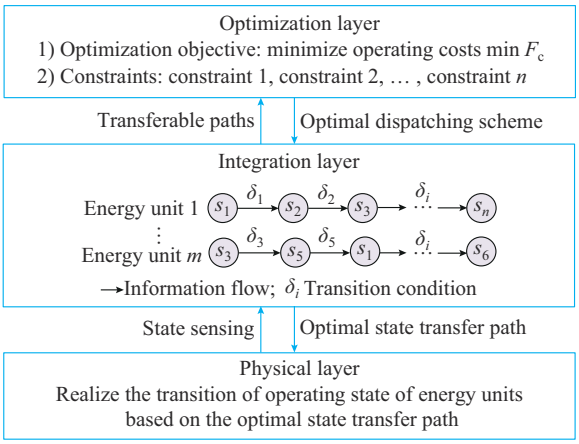


Fig. 2. Hierarchical modeling framework of IES integrated with CPS.

1) Physical layer: this layer integrates the information flow into the physical model of energy unit and establishes an information flow driven state transition model of energy unit.

2) Integration layer: this layer mainly collects the operating states of different energy units $s_i$ in the physical layer to establish the state transition model of the IES and obtains the optimal state transfer path of energy unit according to the optimal dispatch scheme issued by the optimization layer.

3) Optimization layer: this layer considers the operating constraints of the IES and presents the optimization objectives of the IES. It then solves the optimal dispatching scheme based on the optimization objective and sends it to the integration layer.

The physical, integration, and optimization layers interact through information flow. Information flow is achieved by closing the loop of four links: sensing, analysis, decision-making, and execution, as shown in Fig. 3.

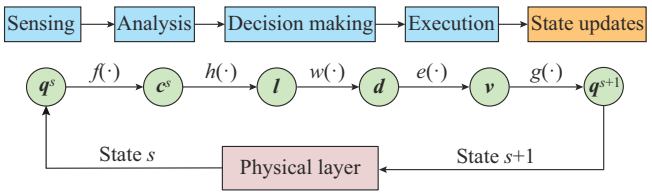


Fig. 3. Interaction between different layers.

In Fig. 3, the operating state of energy unit in the IES can be expressed as $\boldsymbol{q}^s$ in state $s$, which then becomes $\boldsymbol{c}^s$ after sensor sampling. $f(\cdot)$ is the sampling function that converts the operating state of energy unit into the digital signal corresponding to the state sensing link, i.e., the conversion of energy flow into information flow. Then, following the data analysis and processing function $h(\cdot)$, $\boldsymbol{c}^s$ is converted into state data $\boldsymbol{l}$ required by the optimization layer to make decisions. $w(\cdot)$ is the corresponding decision function, which is determined by the optimization algorithm used in the IES, where the corresponding decision result is $\boldsymbol{d}$. $e(\cdot)$ is the function that converts the decision result into the control command, where the conversion result is $\boldsymbol{v}$. $g(\cdot)$ is the function that converts the control command to the next operating state of the energy unit $\boldsymbol{q}^{s+1}$, i.e., the conversion of information flow into energy flow. The state update process shown in Fig. 3 can be expressed as:

$$\boldsymbol{q}^{s+1} = g(e(w(h(f(\boldsymbol{q}^s))))) \tag{1}$$

In summary, the integration layer senses the operating states of energy units in the physical layer through sensors in real time. It then analyzes and processes the information and finally constructs the state transition model of IES-based on the operating state of each energy unit and other historical data to provide $n$ transferable paths for the optimization layer to determine the optimal operation strategy of the IES. The entire state transition trajectory of the IES at different stages can then be observed. Based on different optimization objectives of IES and the transferable path provided by the integration layer, the optimization layer considers the operating constraints of IES, solves the optimal dispatching scheme of the IES, and sends it to the integration layer. The integration layer then obtains the optimal state transfer path of the energy unit according to the optimal dispatching scheme issued by the optimization layer. Based on the optimal state transfer path provided by the integration layer, the physical layer changes the operating state of the energy unit through actuators and completes the conversion of information flow into energy flow. The aforementioned closed-loop process ensures that the traction control of the operating state of the energy unit can be performed according to the optimal state transfer path, thereby enabling the IES to develop in a more optimal direction.

A time delay actually occurs during the process of converting the energy flow into information flow as well as when establishing the state transition model of energy units and the transition between different states in the integration layer. However, the state transition model developed in this study is mainly applied to the day-ahead optimal dispatching of IES, and the time scale (one hour) of day-ahead optimization is longer. This study ignores the time delay in the integration layer because its effects on day-ahead optimal dispatching are negligible. If the state transition model is applied to real-time optimal dispatching of IES, the time delay cannot be ignored because the time scale of real-time optimal dispatching is very short.

## III. IES Modeling Based on CPS

This section details the models of the physical, integration, and optimization layers, as presented in Fig. 2.

### A. Model of Physical Layer

#### 1) Gas Turbine (GT)

The generation efficiency of GT $\eta_{GT}$ is nonlinearly related to the electric load ratio $\lambda_{GT}$, which can be described by the following fourth-order polynomial fitting [23], [24].

$$\begin{cases} \eta_{GT}(t)=\sum_{i=0}^{4}\beta_{GT,i}(\lambda_{GT}(t))^i \\ \alpha_{GT}(t)=\sum_{i=0}^{2}\beta_{\alpha,i}(\lambda_{GT}(t))^i \\ \lambda_{GT}(t)=\dfrac{P_{GT}(t)}{P_{GTN}} \end{cases} \tag{2}$$

where $i$ is the fitting order; $\beta_{GT,i}$ and $\beta_{\alpha,i}$ are the $i^{th}$ order fitting coefficients of GT; $\alpha_{GT}(t)$ is the thermoelectric ratio at time $t$; $P_{GT}(t)$ is the electric power generated by GT at time $t$; and $P_{GTN}$ is the rated electric power of GT. The power generated by GT can then be obtained as:

$$\begin{cases} P_{GT}(t)=F_{GT}(t)\eta_{GT}(t)L_{NG} \\ Q_{GT}(t)=\alpha_{GT}(t)P_{GT}(t) \end{cases} \tag{3}$$

where $Q_{GT}(t)$ is the thermal power generated by GT at time $t$; $F_{GT}(t)$ is the natural gas input to GT at time $t$; and $L_{NG}$ is the calorific value of natural gas.

#### 2) Gas Boiler (GB)

The model of GB can be expressed as:

$$\begin{cases} \eta_{GB}(t)=\sum_{i=0}^{1}\beta_{GB,i}(\lambda_{GB}(t))^i \\ Q_{GB}(t)=F_{GB}(t)\eta_{GB}(t)L_{NG} \\ \lambda_{GB}(t)=\dfrac{Q_{GB}(t)}{Q_{GBN}} \end{cases} \tag{4}$$

where $\eta_{GB}(t)$ and $\lambda_{GB}(t)$ are the thermal efficiency and thermal load ratio of GB at time $t$, respectively; $\beta_{GB,i}$ is the $i^{th}$ order fitting coefficient of GB; $Q_{GBN}$ is the rated themal power of GB; $Q_{GB}(t)$ is the thermal power generated by GB at time $t$; and $F_{GB}(t)$ is the natural gas input to GB at time $t$.

#### 3) Absorption Chiller (AC)

The model of AC can be expressed as:

$$\begin{cases} k_{AC}(t)=\sum_{i=0}^{3}\beta_{AC,i}(\lambda_{AC}(t))^i \\ C_{AC}(t)=k_{AC}(t)Q_{AC}(t) \\ \lambda_{AC}(t)=\dfrac{C_{AC}(t)}{C_{ACN}} \end{cases} \tag{5}$$

where $k_{AC}(t)$ and $\lambda_{AC}(t)$ are the conversion efficiency and cold load ratio of AC at time $t$, respectively; $\beta_{AC,i}$ is the $i^{th}$ order fitting coefficient of AC; $C_{ACN}$ is the rated cold power of AC; and $C_{AC}(t)$ and $Q_{AC}(t)$ are the cold power generated and thermal power consumed by AC at time $t$, respectively.

#### 4) Electric Chiller (EC)

The model of EC can be expressed by:

$$\begin{cases} k_{EC}(t)=\sum_{i=0}^{2}\beta_{EC,i}(\lambda_{EC}(t))^i \\ C_{EC}(t)=k_{EC}(t)P_{EC}(t) \\ \lambda_{EC}(t)=\dfrac{C_{EC}(t)}{C_{ECN}} \end{cases} \tag{6}$$

where $k_{EC}(t)$ and $\lambda_{EC}(t)$ are the conversion efficiency and cold load ratio of EC at time $t$, respectively; $\beta_{EC,i}$ is the $i^{th}$ order fitting coefficient of EC; $C_{ECN}$ is the rated cold power of EC; and $C_{EC}(t)$ and $P_{EC}(t)$ are the cold power generated and electric power consumed by the EC at time $t$, respectively.

#### 5) ESU

The model of ESU can be expressed by:

$$\begin{cases} E_i(t+1)=E_i(t)+\left(\eta_{i,c}P_{i,c}(t)-\dfrac{P_{i,d}(t)}{\eta_{i,d}}\right)\Delta t/S_i \\ 0\le P_{i,c}(t)\le v_{i,c}(t)P_{i,c,max} \\ 0\le P_{i,d}(t)\le v_{i,d}(t)P_{i,d,max} \\ v_{i,c}(t)+v_{i,d}(t)\le 1 \\ E_{i,min}\le E_i(t)\le E_{i,max} \\ E_i(0)=E_i(24) \end{cases} \tag{7}$$

where $E_i(t+1)$ and $E_i(t)$ are the stored energies of ESUs at time $t+1$ and $t$, respectively; $E_{i,max}$ and $E_{i,min}$ are the upper and lower limits of stored energy in ESUs, respectively; $P_{i,c}(t)$ and $\eta_{i,c}$ are the charging power and charging efficiency of ESUs at time $t$, respectively; $P_{i,d}(t)$ and $\eta_{i,d}$ are the discharging power and discharging efficiency of ESUs at time $t$, respectively; $P_{i,c,max}$ and $P_{i,d,max}$ are the upper limit of the charging and discharging power of ESUs, respectively; $S_i$ is the rated capacity of ESUs; $v_{i,d}(t)$ and $v_{i,c}(t)$ are binary variables that take only the values of 0 or 1; $\Delta t$ is the time scale of dispatching; and $E_i(0)$ and $E_i(24)$ are the stored energies of ESUs at the beginning and end of dispatching, respectively.

### B. Model of Integration Layer

The integration layer describes different state combinations of energy units in the IES at different operating stages and establishes a state transition model of IES based on CPS. We consider only the modeling of dispatchable energy units in the IES, such as ECUs, ESUs, and ECSUs.

#### 1) State Transition Modeling of Energy Units

1) ECUs

The information flow (information collection, processing and analysis, and decision-making) is integrated into the physical model of energy unit, and the state transition model of ECU is established based on the CPS, as shown in Fig. 4.

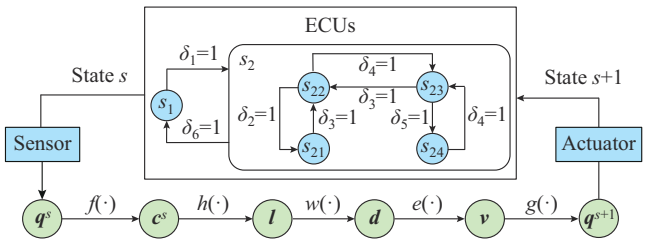


Fig. 4. State transition model of ECU based on CPS.

The operating states of ECU are divided into stopping state $s_1$ and on-load operating state $s_2$. However, in actual operation, an ECU has an obvious partial-load performance; that is, when the ECU is not in operation under rated conditions, its efficiency changes with the load ratio. The efficien-

cy of ECU decreases as the load ratio decreases. For example, the power generation efficiency of GT at a low load ratio is only 80% of that in the full load operation or even lower. In addition, compared with the efficiency of ECU as a constant, the partial-load performance when considering the efficiency of ECU can more accurately and efficiently characterize the operation of ECU, which makes the dispatching scheme of IES more accurate and reasonable. Therefore, in this study, the on-load operating state $s_2$ is divided into four operating states according to its load ratio, i. e., light load state $s_{21}$, medium load state $s_{22}$, heavy load state $s_{23}$, and full load state $s_{24}$, and their energy conversion efficiencies are different. The thresholds for distinguishing the above four operating states are listed in Table I.

TABLE I
THRESHOLDS FOR DISTINGUISHING FOUR OPERATING STATES OF ECUS

| Operating state | Threshold (%) | Operating state | Threshold (%) |
|---|---|---|---|
| $s_{21}$ | $0<\lambda_{GT}<30$ | $s_{23}$ | $80<\lambda_{GT}<100$ |
| $s_{22}$ | $30<\lambda_{GT}<80$ | $s_{24}$ | $\lambda_{GT}=100$ |

Figure 4 shows that the state transition model senses the operating state of ECUs through sensors and changes it through actuators. The following state transfer equations can be established to control the state transition of ECUs between different states.

$$\begin{cases} s_1(t)+s_2(t)=1 \\ s_2(t)=s_{21}(t)+s_{22}(t)+s_{23}(t)+s_{24}(t) \end{cases} \tag{8}$$

$$\begin{cases} y(t)-z(t)=s_1(t)-s_1(t-1) \\ u_1(t)-w_1(t)=s_{21}(t)-s_{21}(t-1) \\ u_2(t)-w_2(t)=s_{22}(t)-s_{22}(t-1) \\ u_3(t)-w_3(t)=s_{23}(t)-s_{23}(t-1) \\ u_4(t)-w_4(t)=s_{24}(t)-s_{24}(t-1) \end{cases} \tag{9}$$

where $y(t)$ and $z(t)$ are the control variables that control the start-up and shut-down of ECUs, respectively; and $u_i(t)$ and $w_i(t)$ are the control variables that control the ECUs to enter and exit the corresponding state, respectively, which are 0-1 variables and cannot be 1 simultaneously. For example, $u_2(t)$ and $w_2(t)$ are 0-1 variables that control the ECUs to enter and exit a medium load operating state, respectively. Equation (8) shows that the ECUs can only be in a unique operating state at time $t$, and (9) indicates the transition constraints for the operating states of ECUs.

The transition between different states of information flow driven ECUs can be achieved by controlling the control variables in (9), where the state transition path of the information flow driven ECUs during the entire optimization period is shown in Fig. 5.

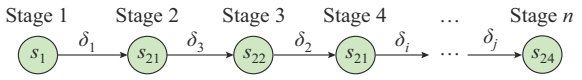


Fig. 5. State transition path of information flow driven ECUs.

The transition conditions $\delta_i$ in Fig. 5 are determined by the control variables in (9), i. e., the values of the control variables are used to trigger the generation of the corresponding $\delta_i$, which causes the ECUs to switch to the desired operating state. An optimization algorithm is used to calculate the control variables in the optimization layer at different time. Table II shows the transition conditions $\delta_i$ between different states of ECU, where $\lambda_n$ is the load ratio of ECU; $\lambda_{min}$ is the minimum load ratio when the ECUs enter state $s_2$; and $\lambda_l$, $\lambda_m$, and $\lambda_h$ are the load ratio thresholds for the ECUs to enter states $s_{22}$, $s_{23}$, and $s_{24}$, respectively.

TABLE II
TRANSITION CONDITIONS BETWEEN DIFFERENT STATES OF ECUS

| Condition | Description | Logical judgment expression |
|---|---|---|
| $\delta_1$ | From $s_1$ to start | $s_1(t)=1\&\&\lambda_n=\lambda_{min}$ |
| $\delta_2$ | Enter $s_{21}$ | $s_2(t)=1\&\&\lambda_{min}<\lambda_n<\lambda_l$ |
| $\delta_3$ | Enter $s_{22}$ | $s_2(t)=1\&\&\lambda_l\le\lambda_n<\lambda_m$ |
| $\delta_4$ | Enter $s_{23}$ | $s_2(t)=1\&\&\lambda_m\le\lambda_n<\lambda_h$ |
| $\delta_5$ | Enter $s_{24}$ | $s_2(t)=1\&\&\lambda_n=\lambda_h$ |
| $\delta_6$ | From $s_2$ to $s_1$ | $s_2(t)=1\&\&\lambda_n<\lambda_{min}$ |

When the logical judgment expression in Table II holds, $\delta_i$ equals 1 and triggers the state transition; otherwise, it equals 0. For example, $\delta_6$ indicates that the ECUs in state $s_2$ enter the state $s_1$ when its load ratio $\lambda_n$ is lower than $\lambda_{min}$, thus effectively avoiding the unreasonable operating state of ECUs with a low load ratio.

2) ESUs

The ESUs include battery storage (BS), thermal storage (TS), and cold storage (CS). According to the mathematical model of ESU [25], its state transition model is established based on CPS, as shown in Fig. 6. The operating state of ESUs is divided into five parts: one stopping state $s_3$, charging state $s_4$, idle state $s_5$, discharging state $s_6$, and another stopping state $s_7$.

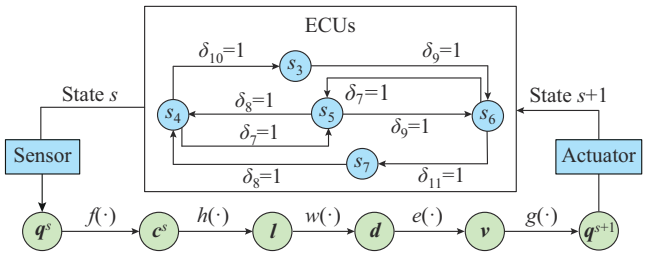


Fig. 6. State transition model of ESU based on CPS.

Similarly, the state transfer equations of ESU similar to those of GT in Fig. 4 can be obtained, which will not be repeated here. Taking BS as an example, the transition conditions between different states are listed in Table III, where $P_e$ is the electric load power; and $P_{in}$ is the power input of the electric load. For example, $\delta_7$ indicates that the BS enters the idle state $s_5$ when its stored energy is in the range of the maximum and minimum values, and there is no surplus power in the IES.

$P_{in}$ can be expressed as:

$$P_{in}(t)=P_{PV}(t)+P_{WT}(t)+P_{GT}(t)+v_b(t)P_{GB}(t)-v_s(t)P_{GS}(t)-P_{EC}(t) \tag{10}$$

TABLE III
TRANSITION CONDITIONS BETWEEN DIFFERENT STATES OF ESUS

| Condition | Description | Logical judgment expression |
|---|---|---|
| $\delta_7$ | Enter $s_5$ | $E_{i,\min} \le E_i(t) \le E_{i,\max} \&\& P_{\text{in}} = P_{\text{e}}$ |
| $\delta_8$ | Enter $s_4$ | $E_i(t) \le E_{i,\max} \&\& P_{\text{in}} > P_{\text{e}}$ |
| $\delta_9$ | Enter $s_6$ | $E_i(t) \ge E_{i,\min} \&\& P_{\text{in}} < P_{\text{e}}$ |
| $\delta_{10}$ | Enter $s_3$ | $s_4(t) = 1 \&\& E_i(t) \ge E_{i,\max}$ |
| $\delta_{11}$ | Enter $s_7$ | $s_6(t) = 1 \&\& E_i(t) \le E_{i,\min}$ |

where $v_{\text{b}}(t)$ and $v_{\text{s}}(t)$ are the 0-1 binary variables, which indicate purchasing and selling electricity from and to the power grid, respectively; $P_{\text{PV}}(t)$ is the output power of photovoltaic (PV); $P_{\text{WT}}(t)$ is the output power of wind turbine (WT); $P_{\text{GB}}(t)$ is the power purchased from power grid; and $P_{\text{GS}}(t)$ is the power sold to power grid.

3) ECSUs

The ECSUs can be classified as critical, shiftable, transferable, and interruptible loads. Part of loads can be transferred moderately under the condition of satisfying IES constraints, which can play the role of peak-shaving and valley-filling, called demand response (DR). In this part, the DR of electric load is considered, and thus an ECSU can be divided into two operating states: normal operating state $s_8$ and transferable operating state $s_9$. The state transition model of ECSU is established based on CPS, as shown in Fig. 7.

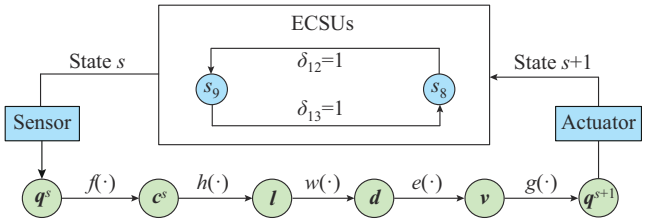


Fig. 7. State transition model of ECSU based on CPS.

The state transition of an ECSU is determined by the time-of-use prices, i.e., the electric load is transferred from high to low electricity price periods. Therefore, the transition condition $\delta_{12}$, as shown in Fig. 7, is set to be 1 during the high electricity price periods, and the transition condition $\delta_{13}$ is set to be 1 during the low electricity price periods.

*2) State Transition Modeling of IES*

In this study, the operating states of IES are divided into shut-down state $s_{\text{sd}}$, start-up state $s_{\text{su}}$, dispatchable state $s_{\text{dis}}$, and fault state $s_{\text{fau}}$. The state transition model of IES, as shown in Fig. 8, is established to illustrate the transition between different states.

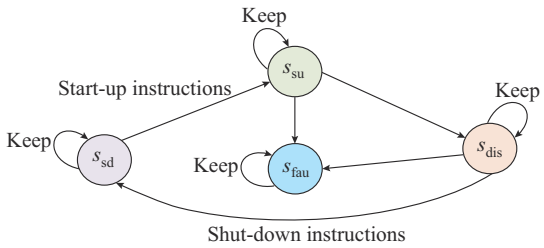


Fig. 8. State transition model of IES.

In general, an IES mainly operates in the dispatchable state to ensure the energy supply quality and to improve the economical operation of IES; therefore, in this study, we mainly consider the dispatchable state of IES. Because the PV and WT are non-dispatchable units, $n$ dispatchable operating states of IES ($s_{\text{m1}}$ - $s_{\text{m}n}$) are shown in Fig. 9.

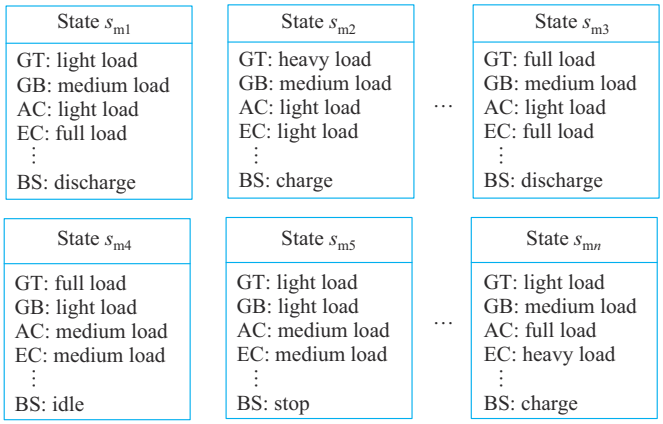


Fig. 9. $n$ dispatchable operating states of IES.

In Fig. 9, each block represents one of the dispatchable operating states of IES and each is obtained by combining the single states of dispatchable units in the IES, e.g., BS, TS, and GT.

The IES can be in any of the aforementioned dispatchable operating states in Fig. 9, and the IES transitions between different operating states over time. Figure 10 shows an example of the state transition of IES between the above $n$ dispatchable operating states, where the actual state transition path depends on the actual operating conditions of the IES.

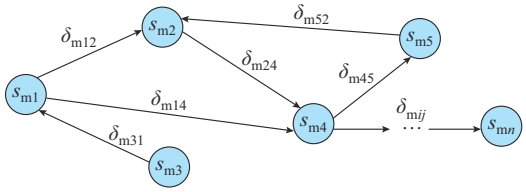


Fig. 10. Example of state transition of IES.

In Fig. 10, $\delta_{\text{m}ij}$ denotes the transition condition of IES from states $s_{\text{m}i}$ to $s_{\text{m}j}$, and its value is determined by the transition conditions of energy unit. For example, $\delta_{\text{m13}}$ is determined by the transition condition that the GT is transferred from a light to a full load state, as shown in Fig. 9. The state transition model of IES observes the entire process of the operating state transition of IES, which is beneficial for designing and selecting the optimal state transition path. For example, to achieve a certain goal, the IES must be transferred from state $s_{\text{m1}}$ to state $s_{\text{m8}}$, assuming that there are $i$ state transition paths ($s_{\text{p1}}$ - $s_{\text{p}i}$) from state $s_{\text{m1}}$ to state $s_{\text{m8}}$, as shown in Fig. 11.

Figure 11 shows the basis of the optimal regulation of the optimization layer. The state transition model provides the transition conditions of energy units between different states as well as multiple state transition paths for the optimization

layer to determine the dispatching scheme of IES when achieving a certain goal. Based on the optimization objective determined by optimization layer and the state transition model of IES, as shown in Fig. 11, the IES performs an analysis and judgment to select an optimal state transition path of IES based on a certain index. One of the indices for selecting the optimal state transition path can be the economic index of IES, such as the minimum operating cost or IES stability.

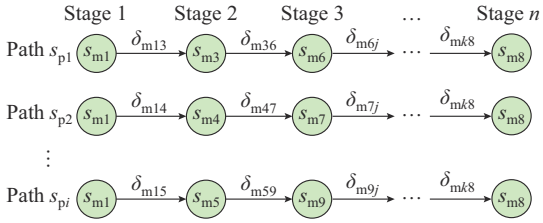


Fig. 11. State transition paths of IES.

In summary, compared with the traditional input-output model of IES, the establishment of state transition model of IES has many advantages: ① the complexity of IES can be reduced by representing its operating control with a set of finite states; ② the observability of IES can be improved by providing a graphical representation of the operating state of energy unit; and ③ a simpler means of modifying the predefined transition conditions to make the IES towards the desired state can be achieved.

### *C. Model of Optimization Layer*

The optimization layer is based on the state transition model given in the integration layer. It considers the constraints to be satisfied by the operation of energy unit and solves the optimal model at the lowest operating cost of IES as the optimization objective.

*1) Objective Function*

The objective function is expressed as:

$$\min F_{\mathrm{c}} = F_{\mathrm{elec}} + F_{\mathrm{gas}} + F_{\mathrm{DR}} \tag{11}$$

where $F_{\mathrm{c}}$ is the total daily operating cost of IES; and $F_{\mathrm{elec}}$, $F_{\mathrm{gas}}$, and $F_{\mathrm{DR}}$ are the cost of purchasing electricity, cost of purchasing gas, and DR cost, respectively, which are expressed as:

$$\begin{cases} F_{\mathrm{elec}} = \sum_{t=1}^{T} (c_{\mathrm{EB},t} P_{\mathrm{GB}}(t) - c_{\mathrm{ES},t} P_{\mathrm{GS}}(t)) \Delta t \\ F_{\mathrm{gas}} = \sum_{t=1}^{T} c_{\mathrm{g},t} \left( \dfrac{P_{\mathrm{GT}}(t)}{\eta_{\mathrm{GT}}(t) L_{\mathrm{NG}}} + \dfrac{Q_{\mathrm{GB}}(t)}{\eta_{\mathrm{GB}}(t) L_{\mathrm{NG}}} \right) \Delta t \\ F_{\mathrm{DR}} = \sum_{t=1}^{T} c_{\mathrm{s}} \left| P_{\mathrm{DR}}(t) \right| \Delta t \end{cases} \tag{12}$$

where $c_{\mathrm{EB},t}$ and $c_{\mathrm{ES},t}$ are the electricity prices of purchasing and selling electricity, respectively; $c_{\mathrm{g},t}$ is the price of natural gas purchased by the IES from the natural gas network; $c_{\mathrm{s}}$ is the load unit compensation cost; $P_{\mathrm{DR}}(t)$ is the amount of load participating in the DR at time $t$; and $T$ is the dispatching period.

*2) Constraints*

The IES must satisfy the energy balance, energy unit output, and power exchange constraints of power grid in operation, which are described in [25] and [26] and will not be repeated here. In addition, the following DR constraint must be satisfied:

$$\begin{cases} \sum_{t=1}^{24} P_{\mathrm{DR}}(t) = 0 \\ 0 \le \left| P_{\mathrm{DR}}(t) \right| \le v_{\mathrm{DR}}(t) P_{\mathrm{load}}(t) \end{cases} \tag{13}$$

where $v_{\mathrm{DR}}(t)$ is the maximum proportion of load change at time $t$; and $P_{\mathrm{load}}(t)$ is the load power at time $t$.

The first constraint in (13) indicates that the total load power before and after the implementation of DR should remain unchanged in one dispatch cycle, i.e., the sum of the DR power should be zero. The second constraint in (13) is used to limit the variation range of the load participating in the DR at a certain time.

The model of the optimization layer in IES composed of the aforementioned objective function and constraints is a mixed-integer nonlinear programming (MINP) problem, and an effective tool called IPOPT is used to solve this kind of optimization problem. Because the IPOPT can only solve continuous programming problems, the optimization model in this study is an MINP problem containing binary variables. For example, for ESUs, the mathematical model in (7) contains two binary variables $v_{i,\mathrm{d}}(t)$ and $v_{i,\mathrm{c}}(t)$, and we can eliminate the binary variables and convert them to the following equivalent form:

$$\begin{cases} 0 \le P_{i,\mathrm{c}}(t) \le P_{i,\mathrm{c,max}} \\ 0 \le P_{i,\mathrm{d}}(t) \le P_{i,\mathrm{d,max}} \\ P_{i,\mathrm{c}}(t) P_{i,\mathrm{d}}(t) = 0 \end{cases} \tag{14}$$

Formula (14) can constrain the ESUs from being charged and discharged simultaneously. Then, after the equivalence of (14), the developed optimization model does not contain binary variables; therefore, it can be solved using the IPOPT.

The solution flow for day-ahead optimal dispatching of the IES is presented in Fig. 12.

1) At the beginning of regulation, the information of energy unit including electric, cold, and thermal power outputs from each energy unit of IES is collected through the sensors, and the parameter information including the gas price, electricity purchase and sale prices, and electric, cold, and thermal loads is obtained through the network.

2) The minimum daily operating cost of IES is selected as the optimization objective, and constraints are set to establish the day-ahead optimal dispatching of IES.

3) Based on the collected data, the computing center solves the day-ahead optimal dispatching model using the IPOPT and generates the optimal control commands.

4) The control system receives the control commands and controls each energy unit to change its operating state along the optimal state transition path.

5) Judge whether the regulation cycle is finished. If not, wait for the next regulation time.

6) The optimization is terminated and the day-ahead optimal dispatching of the IES is output.

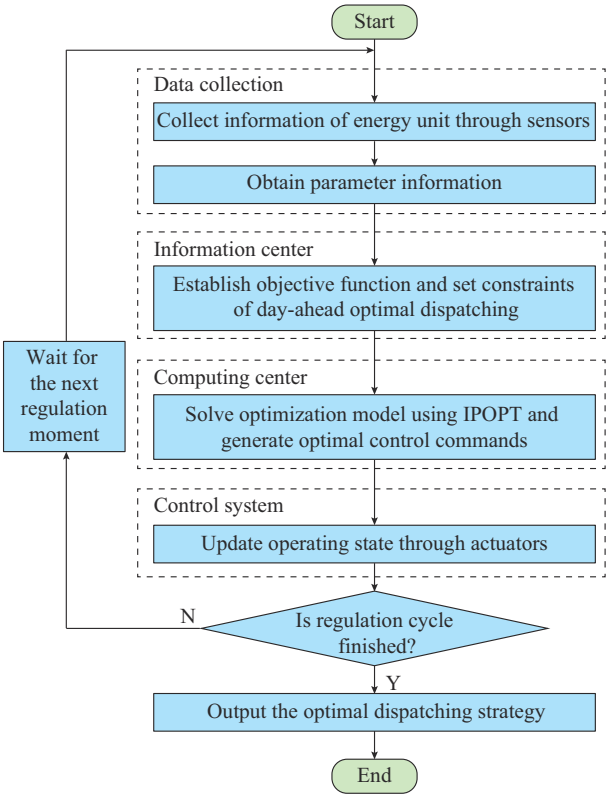


Fig. 12. Solution flow for day-ahead optimal dispatching of IES.

## IV. Case Studies

### A. Parameters for IES

To verify the feasibility of the proposed modeling method, numerical simulations are conducted based on the IES, as shown in Fig. 13, where $P_G$ is the power input to the IES from the power grid; $P_{BS}$ is the output power of BS; $C_{CS}$ is the output cold power of CS; $Q_{TS}$ is the output thermal power of TS; and $L_e$, $L_h$, and $L_c$ are the power of electric, thermal and cold loads, respectively.

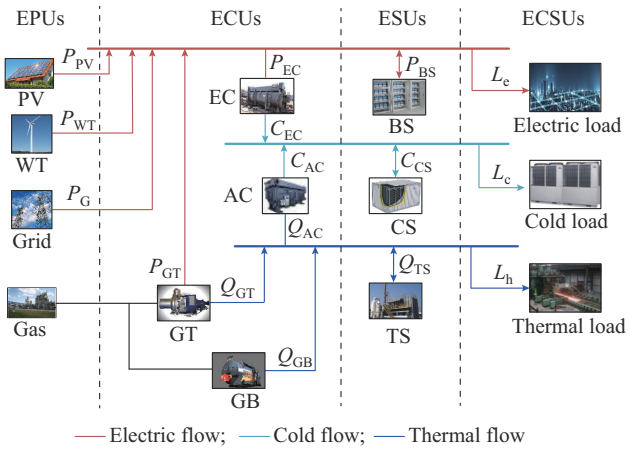


Fig. 13. Structure of IES.

The main parameters of energy unit in IES, as given in Fig. 13, are listed in Table IV, where the subscript max denotes the corresponding maximum values. In this study, the IES exchanges power with the power grid according to the electricity prices during different periods, as listed in Table V.

TABLE IV
Main Parameters of Energy Unit in IES

| Energy unit | Parameter | Value |
|---|---|---|
| GT | $P_{GT,max}$ | 1200 kW |
| | Rated $\eta_{GT}$ | 0.34 |
| | Rated $\alpha_{GT}$ | 1.48 |
| | $\beta_{GT,i}$ | $\beta_{GT,1}=1.11$, $\beta_{GT,2}=-1.64$, $\beta_{GT,3}=1.29$, $\beta_{GT,4}=-0.41$ |
| | $\beta_{\alpha,i}$ | $\beta_{\alpha,0}=1.92$, $\beta_{\alpha,1}=-3.04$, $\beta_{\alpha,2}=1.76$ |
| GB | $Q_{GB,max}$ | 1000 kW |
| | Rated $\eta_{GB}$ | 0.85 |
| | $\beta_{GB,i}$ | $\beta_{GB,0}=0.81$, $\beta_{GB,1}=0.13$ |
| EC | $C_{EC,max}$ | 650 kW |
| | Rated $k_{EC}$ | 3 |
| | $\beta_{EC,i}$ | $\beta_{EC,0}=-0.88$, $\beta_{EC,1}=12.89$, $\beta_{EC,2}=-10.48$ |
| AC | $C_{AC,max}$ | 800 kW |
| | Rated $k_{AC}$ | 1.5 |
| | $\beta_{AC,i}$ | $\beta_{AC,0}=0.12$, $\beta_{AC,1}=2.61$, $\beta_{AC,2}=-0.15$, $\beta_{AC,3}=-1.49$ |

TABLE V
Electricity Prices During Different Periods

| Electricity period | Time interval | Electricity price (¥/kWh) | |
|---|---|---|---|
| | | Purchasing | Selling |
| Peak | Hours 8-12<br>Hours 19-23 | 1.12 | 1.18 |
| Flat | Hours 12-19 | 0.84 | 0.84 |
| Valley | Hours 23-8 | 0.35 | 0.28 |

Figure 14 shows the actual data curves of loads on a certain day.

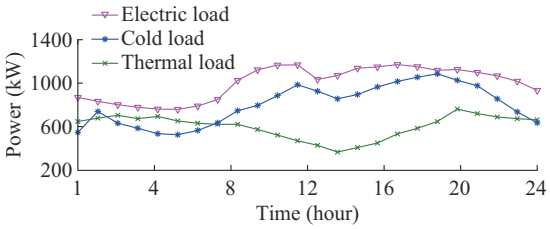


Fig. 14. Actual data curves of loads on a certain day.

Based on the parameters in Table IV, a fitted curve of the conversion efficiency for ECUs can be obtained, as shown in Fig. 15.

### B. Analysis and Discussion of Optimization Results

#### 1) Comparison with Traditional Modeling Method

To test the superiority of the proposed modeling method, two cases are considered for comparison.

1) Case 1: the optimal dispatching of IES based on the proposed modeling method of IES based on CPS.

2) Case 2: the optimal dispatching of IES based on the traditional modeling method of EH.

Note that both cases do not consider the DR.

Figure 16 shows the optimal dispatching results of the electric power in Cases 1 and 2, where $P_{\mathrm{BS,c}}$ and $P_{\mathrm{BS,d}}$ are the charging and discharging power of BS, respectively. This figure shows that in Case 1, during the valley periods, most of the electric load is supplied by the power grid while the BS is charged. During the peak periods, the electric load is mainly supplied by the GT and BS, whereas the redundant electric power generated in the IES is sold to the power grid to reduce the operating costs of IES. The output of GT is also affected by the thermal load demand in the IES, and the GT operates at full load when the thermal load demand exceeds the thermal power generated by the GT.

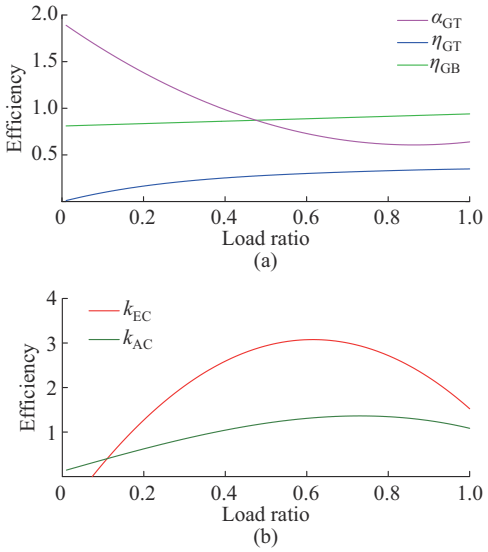


Fig. 15. Fitting curve of conversion efficiency for ECUs. (a) GT and GB. (b) EC and AC.

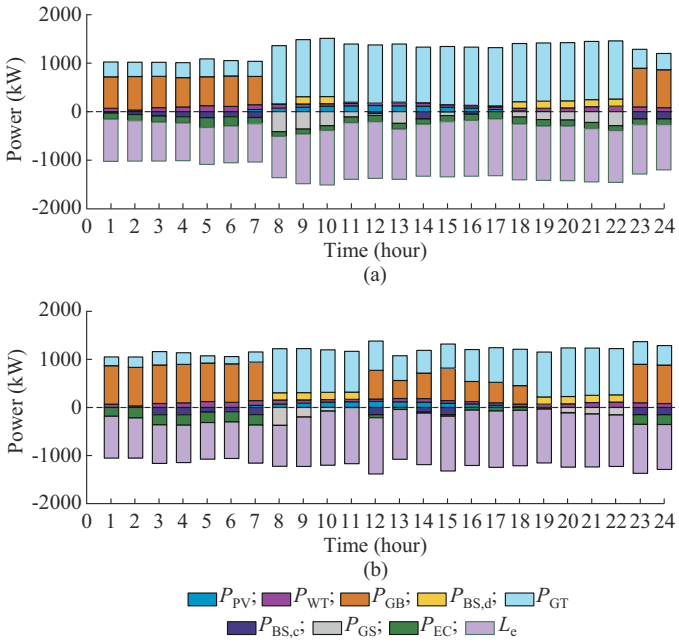


Fig. 16. Optimal dispatching results of electric power. (a) Case 1. (b) Case 2.

In Case 2, for each energy unit, the optimal dispatching results are similar to those in Case 1. The sole difference during the flat periods is: the electric load in Case 1 is supplied by the GT, whereas that in Case 2 is supplied by both the GT and power grid. This is mainly because the traditional modeling method considers the conversion efficiency of the energy unit as the rated efficiency, which is generally the optimal operating point of the energy unit with the highest operating efficiency. However, due to the limitations of the thermal load and thermal electricity ratio, the GT fails to supply all of electric loads in Case 1.

Figure 17 shows optimal dispatching results of the thermal power in Cases 1 and 2, where $Q_{\mathrm{TS,d}}$ and $Q_{\mathrm{TS,c}}$ are the heat released and absorbed by the TS, respectively. The results show that the outputs of each energy unit in these two cases are different. The thermal load in Case 1 is mainly supplied by the GT and GB, whereas in Case 2, it is mainly supplied by the GT during most periods, and the GB only supplies energy during the peak periods.

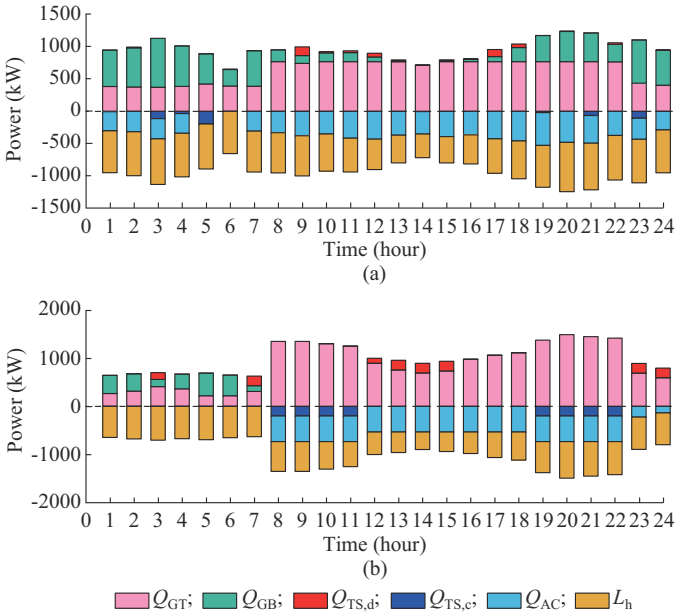


Fig. 17. Optimal dispatching results of thermal power. (a) Case 1. (b) Case 2.

The operating state of energy unit is considered in Case 1. When the electricity price and thermal load are determined, the optimal dispatching result is related to the load ratio of energy unit. When the thermal load is small, both the GT and GB are at low load levels, and their operating efficiencies are lower than those operate at full load. However, because the GT can generate both electric and thermal energy, it is more economical than GB at a low load level. Therefore, the GT is used to meet the thermal load demand during hours 12-16. When the thermal load increases, the thermal energy generated by the GT cannot satisfy the thermal load and the thermal output of GB gradually increases and its efficiency is at a high load level. At hour 3, the GB covers the main thermal load demand. However, during the peak periods, the GT operates at full load due to the increase in electricity purchase cost. Therefore, the thermal load is mainly

supplied by the GT, and the insufficient thermal load is supplied by the GB. The TS releases heat during periods of insufficient heat and stores it during periods of excess heat.

By contrast, Case 2 does not consider the operating state of energy unit, where the conversion efficiency of energy unit is considered as rated efficiency. Under the rated efficiency, the GT is more economical, so GT is used as the main thermal energy unit. GB and TS are used for supplying the thermal load during peak thermal load periods when the GT is undersupplied. During the valley periods, the electric load is mainly supplied by the power grid. Therefore, the output of GT is reduced, and the lacking thermal load is supplied by the GB and TS.

Figure 18 shows the optimal dispatching results of the cold power in Cases 1 and 2, where $C_{CS,d}$ and $C_{CS,c}$ are the cold energy released and absorbed by CS, respectively. We can observe that the cold load is mainly supplied by the EC and AC. In addition, the output of EC is mainly affected by the electricity price, whereas the output of AC is mainly affected by the heat generated by IES. Unlike GB and GT, the efficiency curves of EC and AC in Case 1 are inverted U-shaped, with the best efficiency at partial load points. During the valley periods, the economy of cooling supply by EC is high. Therefore, the EC covers most of the cold load. During the peak periods, the IES generates more heat, and the economy of AC is gradually improved. Thus, the output of AC gradually increases.

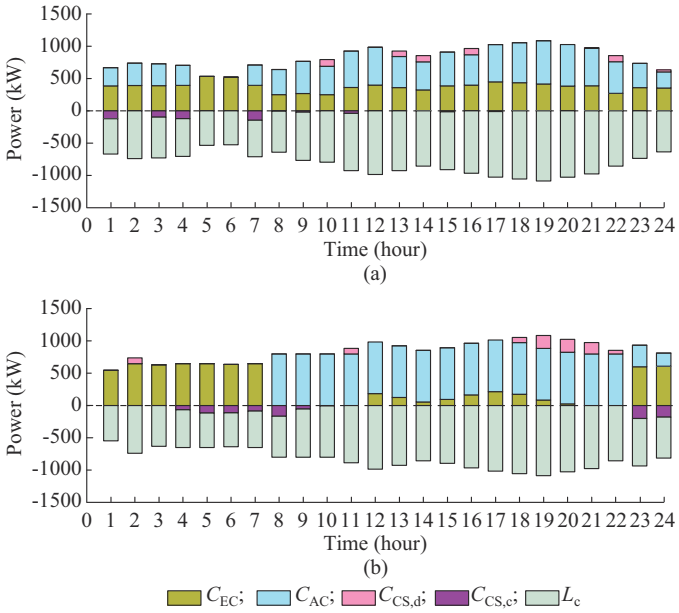


Fig. 18. Optimal dispatching results of cold power. (a) Case 1. (b) Case 2.

In Case 2, during the valley periods, the EC covers the entire cold load. During the peak periods, the AC covers most of the cold load, and an insufficient part is provided by CS.

It is worth noting that the conversion efficiency of the energy unit in Case 2 is regarded as the rated efficiency, which is the desired dispatching scheme. However, the actual conversion efficiency of energy unit is usually not the rated value. Therefore, the optimal dispatching results obtained in Case 2 often exhibit large errors, resulting in a shortage of load supply in actual operation. Figure 19 shows the shortages of electric, thermal, and cold power during each period in Case 2.

Figure 19 shows that there is a source-load mismatch in the actual operation in Case 2. At this time, the energy unit output must be corrected, i. e., an insufficient load is supplied by the power grid and gas network, resulting in an increase in the operating cost of IES. To verify this conclusion, the operating costs in Cases 1 and 2 are calculated, as listed in Table VI.

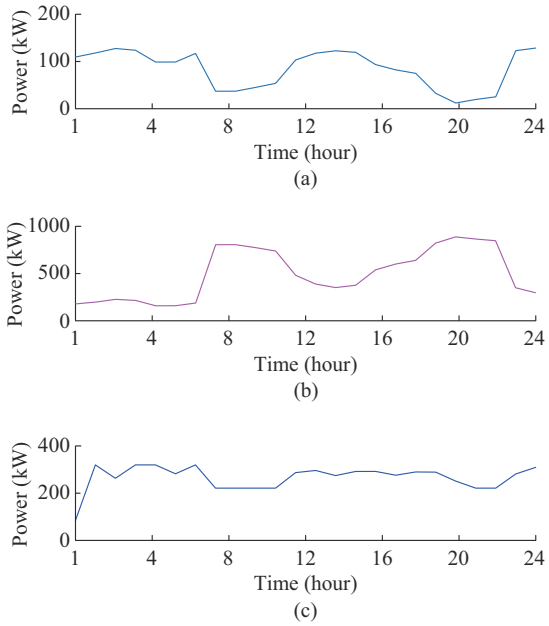


Fig. 19. Shortages of electric, thermal, and cold power during each period in Case 2. (a) Electric power. (b) Thermal power. (c) Cold power.

TABLE VI
OPERATING COSTS IN CASES 1 AND 2

| Case | Operating cost (¥) |
|---|---|
| 1 | 24603 |
| 2 | 19014 (ideal); 25133 (actual) |

As can be observed from Table VI, because Case 2 considers the conversion efficiency of the energy unit as the rated efficiency, less natural gas is required to generate the same amount of energy, resulting in a lower ideal operating cost in Case 2. Table VI also shows that, in Case 2, the actual operating cost increases by 32.1% over that of the ideal operating cost. This is mainly because the traditional modeling method considers the conversion efficiency of the energy unit as the rated efficiency, which generates an overestimation over the operating efficiency of energy unit and often causes the energy unit to operate at a low load level. A comparison of the operating cost in Case 1 and the actual operating cost in Case 2 reveals that the proposed modeling method reduces the operating cost by 2.1%, mainly because the state transition model of IES can accurately and efficiently characterize the operation of energy unit. These results show

that the proposed modeling method achieves a refined description for the operating state of energy unit. Thus, the obtained optimization results are more consistent with actual situations.

*2) Comparison of Load Ratios Under Different Modeling Methods*

Figure 20 shows the load ratio of each energy unit in Cases 1 and 2. It can be observed that the load ratios of both GT and GB are improved in Case 1 compared with those in Case 2, which verifies the proposed modeling method can achieve a refined description for the operating state of energy unit. Because the conversion efficiencies of GT and GB are positively related to the load ratio, they are improved in Case 1 compared with in Case 2. By contrast, the operating efficiency curves of EC and AC are inverted U-shaped, i.e., the optimal operating efficiencies of EC and AC are located in the part load region. Therefore, the EC and AC can operate in a more efficient load ratio interval in Case 1.

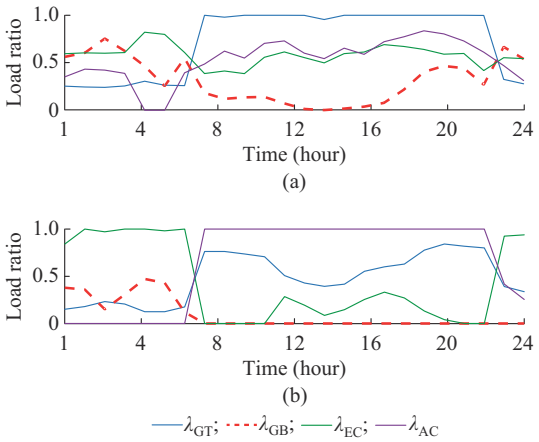


Fig. 20. Load ratio of each energy unit in Cases 1 and 2. (a) Case 1. (b) Case 2.

In addition, the proposed modeling method of CPS realizes the observability for the operating state of energy unit and its state transition process in one dispatch cycle. Figure 21 shows the state transition processes of ECU and ESU.

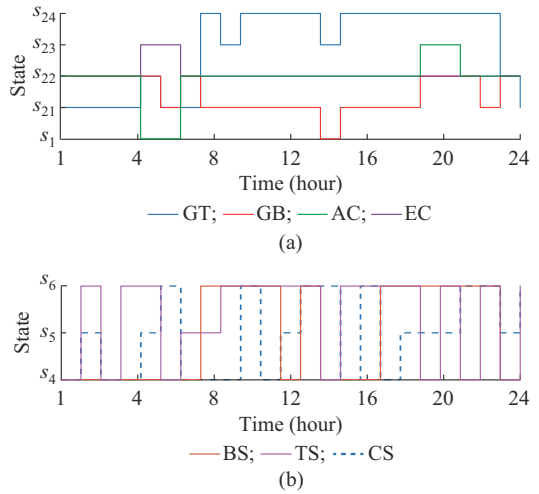


Fig. 21. State transition processes of ECU and ESU. (a) ECU. (b) ESU.

Figure 21 shows that the proposed modeling method of CPS realizes the judgment of the operating state of energy unit throughout the optimization period and can reveal the operating state of energy unit at each moment as well as the duration of energy unit under this operating state. These are conducive to a reasonable configuration of the energy unit in the IES. The duration of energy unit under different operating states in Case 1 is given in Table VII.

TABLE VII
DURATION OF ENERGY UNIT UNDER DIFFERENT OPERATING STATES IN CASE 1

| Energy unit | Duration under different operating states (hour) | | | | |
|---|---|---|---|---|---|
| | Stopping | Light load | Medium load | Heavy load | Full load |
| GT | 0 | 7 | 2 | 0 | 15 |
| GB | 0 | 13 | 11 | 0 | 0 |
| EC | 0 | 0 | 24 | 0 | 0 |
| AC | 2 | 0 | 20 | 2 | 0 |

In summary, the proposed modeling method of CPS can visualize the operating state of energy unit and its state transition, and the operating state of energy unit can be controlled according to the planned transfer path to achieve the optimal state and state transition of energy unit.

*3) Optimal Dispatch Results with Considering DR*

Considering the characteristics of thermal and cold loads, it is difficult to change the users' habits. Therefore, we consider only the DR of electric load. Figure 22 shows the electric load curve with and without considering DR.

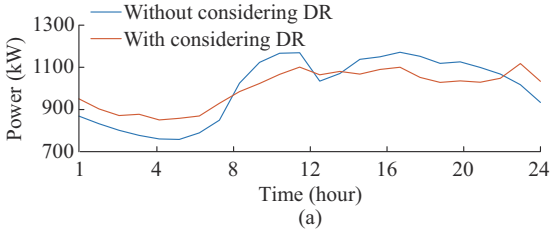


Fig. 22. Electric load curves with and without considering DR.

Figure 22 shows that, with considering DR, the electric load during the peak period shifts to a lower period due to the time-of-use prices, which achieves peak-shaving and valley-filling. To analyze the effects of DR on optimal dispatching, Cases 3 and 4 are set up for comparison.

1) Case 3: the proposed modeling method without considering DR.

2) Case 4: the proposed modeling method with considering DR.

Figure 23 shows the optimal dispatch results of IES in Case 4. The analysis of the optimal dispatch results in Case 3 is the same as that in Case 1. Figure 23 shows that the output power curve trend of ECU in Case 4 is essentially the same as that in Case 1. The difference is that the implementation of DR changes the output of ECU at each moment. For example, for the electric load, the implementation of DR causes the load to shift from the peak periods to valley peri-

ods. Therefore, during the valley periods, the IES purchases more power to meet the electric load in Case 4 compared with Case 3, as shown in Fig. 23(a). During the peak periods, the GT operates at full load and the reduction of load during the peak periods causes more electricity to be sold to the power grid to reduce the operating costs of IES. For the thermal and cold loads, although they are not shifted, the implementation of DR also affects the output of thermal and cold energy unit. However, the overall trend in Case 4 is basically the same as that of Case 3. For the ESU, because the charging and discharging states of BS are mainly affected by the electricity price, the charging and discharging rules of BS in Case 4 are similar to those in Case 3. However, the output of BS during each period varies due to the effects of DR. Because the implementation of DR changes the output of thermal and cold energy units, the charging and discharging rules of TS and CS in Case 4 are different from those in Case 3.

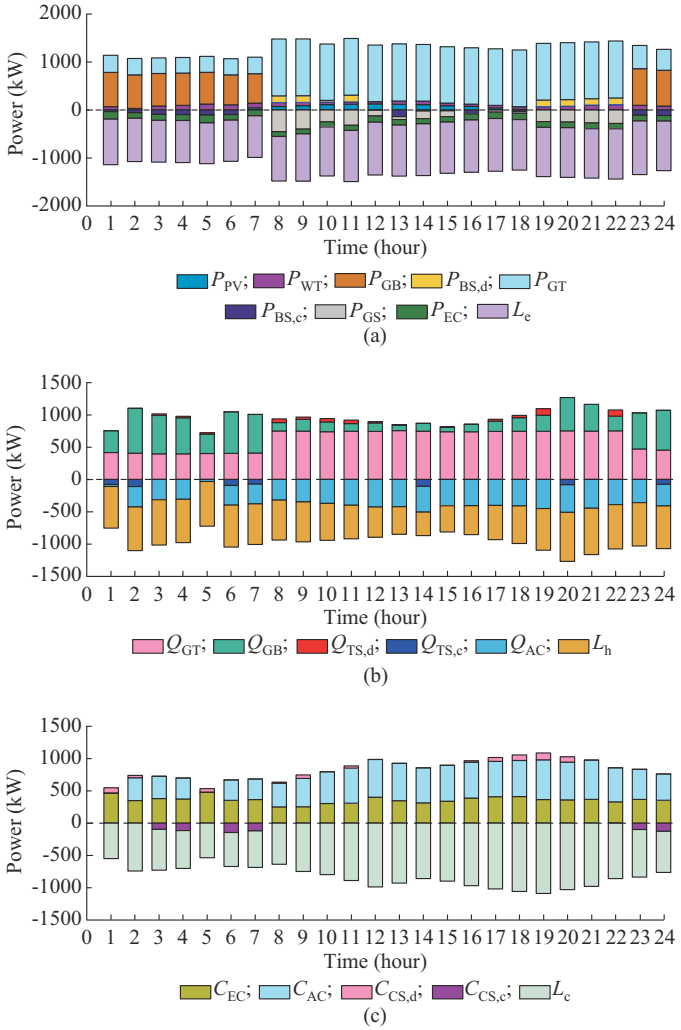


Fig. 23. Optimal dispatch results of IES in Case 4. (a) Electric power. (b) Thermal power. (c) Cold power.

Table VIII lists the operating costs in Cases 3 and 4. The operating cost of IES is lower after the implementation of DR. This is mainly because the implementation of DR shifts the electric load from the peak hours to flat ones, reducing the cost of purchasing electricity and gas. Although the DR cost increases, the total operating cost decreases.

TABLE VIII
OPERATING COSTS IN CASES 3 AND 4

| Case | Cost of purchasing gas and electricity (¥) | DR cost (¥) | Total operating cost (¥) |
|---|---|---|---|
| 3 | 24603.0 | 0 | 24603 |
| 4 | 22887.8 | 358.2 | 23246 |

*4) Effects of DR on Operating Efficiency of Energy Unit*

For a further analysis of the effects of DR on the optimal dispatch of IES, the efficiency curves of ECU in Cases 3 and 4 are shown in Fig. 24.

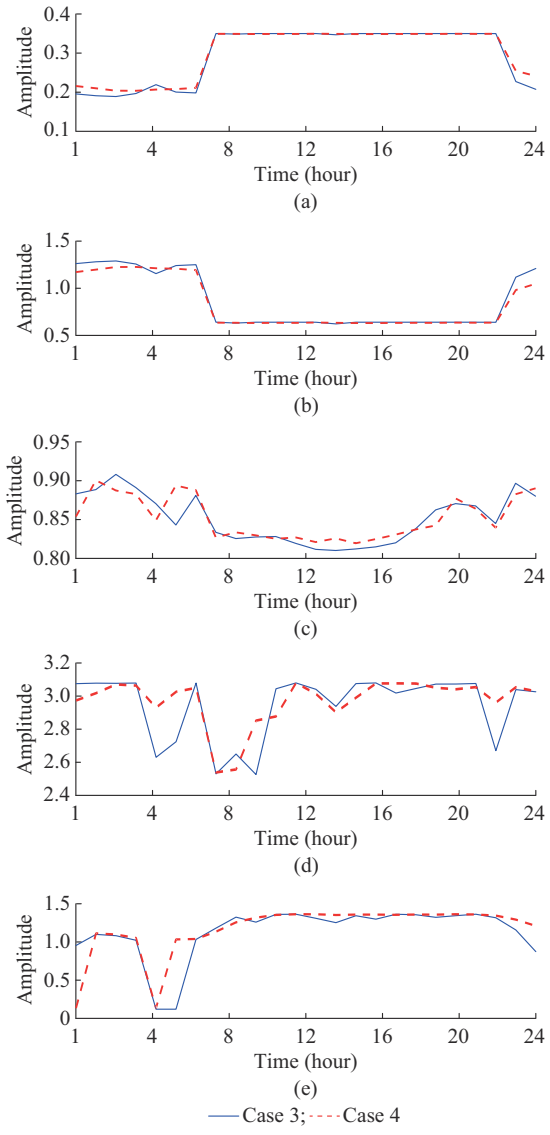


Fig. 24. Efficiency curves of ECU in Cases 3 and 4. (a) $\eta_{GT}$. (b) $\alpha_{GT}$. (c) $\eta_{GB}$. (d) $k_{EC}$. (e) $k_{AC}$.

As shown in Fig. 24(a) and (b), $\eta_{GT}$ and $\alpha_{GT}$ in Cases 3 and 4 are basically the same during most of periods. Affected by the DR, $\eta_{GT}$ in Case 4 is higher during periods 1-7 and 23-24, i.e., more electricity can be generated by consum-

ing the same volume of natural gas, which is beneficial to the economical operation of the IES. In addition, because $\alpha_{GT}$ is inversely related to the load ratio, $\alpha_{GT}$ in Case 4 is lower than that in Case 3 during hours 1-7 and 23-24.

As shown in Fig. 24(c), the trends of $\eta_{GB}$ in Cases 3 and 4 are basically the same. The electric load is shifted from the peak periods to hours 3-5 due to DR, and the output of GT increases, whereas the output of GB decreases. Because $\eta_{GB}$ is positively related to the load ratio, $\eta_{GB}$ during hours 3-5 in Case 4 is slightly lower than that in Case 3. However, during most of other periods, $\eta_{GB}$ in Case 4 is higher than that in Case 3.

The operating efficiency curves of EC and AC are inverted as U-shaped. With an increase in the load ratio, the operating efficiencies of EC and AC first increase and then decrease, i.e., the best operating efficiencies of EC and AC are in the partial load region. As shown in Fig. 24(d) and (e), the operating efficiencies of EC and AC in Case 4 are basically the same as those in Case 3 during most of periods. However, the operating efficiencies of EC and AC in Case 4 are higher than those in Case 3.

In summary, the implementation of DR can further improve the operating interval and overall efficiency of energy unit, and reduce the energy loss of the IES.

## V. Conclusion

This study proposes a state transition modeling method of IES based on a CPS, and the feasibility of the proposed modeling method is verified through case studies. The main conclusions are as follows.

1) The proposed state transition model can visualize the regulation of the operating state and state transition of the energy unit. It can also identify the operating state of the energy unit at each moment and the duration of the energy unit under a given operating state, which is conducive to the reasonable configuration of the energy unit in the IES.

2) The proposed state transition model can accurately and efficiently characterize the energy unit operation, which makes the dispatching scheme of IES more accurate and reasonable and reduces the operating costs of IES by 2.1%.

3) The implementation of DR further improves the operating points of energy unit, enabling it to operate in a more efficient load ratio range while improving the overall efficiency of IES.

As the number of energy units in an IES increases, the proposed state transition model will have irreplaceable advantages. Future research will consider the effects of additional factors on the operating state of energy unit and further refine the state transition model of the energy unit to improve the optimal dispatching method proposed in this study.

## Reference


[1] W. Liao, S. Wang, B. Bak-Jensen *et al*., "Ultra-short-term interval prediction of wind power based on graph neural network and improved bootstrap technique," *Journal of Modern Power Systems and Clean Energy*, vol. 11, no. 4, pp. 1100-1114, Jul. 2023.

[2] C. Wang, Z. Wang, S. Chu *et al*., "A two-stage underfrequency load shedding strategy for microgrid groups considering risk avoidance," *Applied Energy*, vol. 367, p. 123343, Aug. 2024.

[3] Z. Zhao, J. Xu, J. Guo *et al*., "Robust energy management for multi-microgrids based on distributed dynamic tube model predictive control," *IEEE Transactions on Smart Grid*, vol. 15, no. 1, pp. 203-217, Jan. 2024.

[4] Y. Yang, P. Yang, Z. Zhao *et al*., "An adaptive optimal scheduling strategy for islanded micro-energy grid considering the multiple system operating states," *IEEE Transactions on Sustainable Energy*, vol. 14, no. 1, pp. 393-408, Jan. 2023.

[5] Q. Cui, J. Zhu, J. Shu *et al*., "Comprehensive evaluation of electric power prediction models based on D-S evidence theory combined with multiple accuracy indicators," *Journal of Modern Power Systems and Clean Energy*, vol. 10, no. 3, pp. 597-605, May 2022.

[6] T. Ma, J. Wu, and L. Hao, "Energy flow modeling and optimal operation analysis of the micro energy grid based on energy hub," *Energy Conversion and Management*, vol. 133, pp. 292-306, Feb. 2017.

[7] L. Tian, L. Cheng, J. Guo *et al*., "System modeling and optimal dispatching of multi-energy microgrid with energy storage," *Journal of Modern Power Systems and Clean Energy*, vol. 8, no. 5, pp. 809-819, Sept. 2020.

[8] B. Chen, Q. Guo, G. Yin *et al*., "Energy-circuit-based integrated energy management system: theory, implementation, and application," *Proceedings of the IEEE*, vol. 110, no. 12, pp. 1897-1926, Dec. 2022.

[9] T. Liu, D. Zhang, H. Dai *et al*., "Intelligent modeling and optimization for smart energy hub," *IEEE Transactions on Industrial Electronics*, vol. 66, no. 12, pp. 9898-9908, Dec. 2019.

[10] P. Li, W. Sheng, Q. Duan *et al*., "A Lyapunov optimization-based energy management strategy for energy hub with energy router," *IEEE Transactions on Smart Grid*, vol. 11, no. 6, pp. 4860-4870, Nov. 2020.

[11] Y. Cao, W. Wei, J. Wang *et al*., "Capacity planning of energy hub in multi-carrier energy networks: a data-driven robust stochastic programming approach," *IEEE Transactions on Sustainable Energy*, vol. 11, no. 1, pp. 3-14, Jan. 2020.

[12] L. Wang, C. Hou, B. Ye *et al*., "Optimal operation analysis of integrated community energy system considering the uncertainty of demand response," *IEEE Transactions on Power Systems*, vol. 36, no. 4, pp. 3681-3691, Jul. 2021.

[13] D. Xu, Q. Wu, B. Zhou *et al*., "Distributed multi-energy operation of coupled electricity, heating, and natural gas networks," *IEEE Transactions on Sustainable Energy*, vol. 11, no. 4, pp. 2457-2469, Oct. 2020.

[14] C. Deng, Y. Wang, C. Wen *et al*., "Distributed resilient control for energy storage systems in cyber-physical microgrids," *IEEE Transactions on Industrial Informatics*, vol. 17, no. 2, pp. 1331-1341, Feb. 2021.

[15] S. Xin, Q. Guo, H. Sun *et al*., "Cyber-physical modeling and cyber-contingency assessment of hierarchical control systems," *IEEE Transactions on Smart Grid*, vol. 6, no. 5, pp. 2375-2385, Sept. 2015.

[16] L. Xu, Q. Guo, Z. Wang *et al*., "Modeling of time-delayed distributed cyber-physical power systems for small-signal stability analysis," *IEEE Transactions on Smart Grid*, vol. 12, no. 4, pp. 3425-3437, Jul. 2021.

[17] H. Ye, K. Liu, Q. Mou *et al*., "Modeling and formulation of delayed cyber-physical power system for small-signal stability analysis and control," *IEEE Transactions on Power Systems*, vol. 34, no. 3, pp. 2419-2432, May 2019.

[18] L. Xu, Q. Guo, T. Yang *et al*., "Robust routing optimization for smart grids considering cyber-physical interdependence," *IEEE Transactions on Smart Grid*, vol. 10, no. 5, pp. 5620-5629, Sept. 2019.

[19] B. Ti, J. Wang, G. Li *et al*., "Operational risk-averse routing optimization for cyber-physical power systems," *CSEE Journal of Power and Energy Systems*, vol. 8, no. 3, pp. 801-811, May 2022.

[20] B. Ti, G. Li, M. Zhou *et al*., "Resilience assessment and improvement for cyber-physical power systems under typhoon disasters," *IEEE Transactions on Smart Grid*, vol. 13, no. 1, pp. 783-794, Jan. 2022.

[21] G. Cao, W. Gu, P. Li *et al*., "Operational risk evaluation of active distribution networks considering cyber contingencies," *IEEE Transactions on Industrial Informatics*, vol. 16, no. 6, pp. 3849-3861, Jun. 2020.

[22] H. Gao, X. Lyu, S. He *et al*., "Integrated planning of cyber-physical active distribution system considering multidimensional uncertainties," *IEEE Transactions on Smart Grid*, vol. 13, no. 4, pp. 3145-3159, Jul. 2022.

[23] M. Bianchi, A. D. Pascale, F. Melino *et al*., "Performance prediction of micro-CHP systems using simple virtual operating cycles," *Applied Thermal Engineering*, vol. 71, no. 2, pp. 771-779, Oct. 2014.

[24] T. Zakrzewski and B. Stephens, "Updated generalized natural gas reciprocating engine part-load performance curves for cogeneration applications," *Science and Technology for the Built Environment*, vol. 23,

no. 7, pp. 1151-1158, Oct. 2017.
[25] Y. Yang, P. Yang, Z. Zhao *et al*., "A multi-timescale coordinated optimization framework for economic dispatch of micro-energy grid considering prediction error," *IEEE Transactions on Power Systems*, vol. 39, no. 2, pp. 3211-3226, Mar. 2024.
[26] Y. Yang, G. Lu, Z. Li *et al*., "A hierarchical modeling framework for cyber-physical micro energy grid system," *Frontiers in Energy Research*, vol. 9, p. 775469, Dec. 2021.

**Yi Yang** received the M.S. degree in electrical engineering from Hunan University, Changsha, China, in 2018, and the Ph.D. degree in electrical engineering from South China University of Technology, Guangzhou, China, in 2023. He is currently a Lecturer with the College of Electrical Engineering and New Energy, China Three Gorges University, Yichang, China. His research interests include power electronics for microgrid, integrated energy system optimization, and power cyber-physical system.

**Peng Zhang** received the B.S. degree in electrical engineering from Hubei Engineering University, Xiaogan, China, in 2023. He is currently pursuing the master's degree in the College of Electrical Engineering and New Energy, China Three Gorges University, Yichang, China. His research interests include integrated energy system optimization and power cyber-physical system.

**Can Wang** received the B.S. and M.S. degrees in control theory and engineering from Wuhan University of Science and Technology, Wuhan, China, in 2010 and 2013, respectively, and the Ph.D. degree in electrical engineering from South China University of Technology, Guangzhou, China, in 2017. He is currently an Associate Professor of electrical engineering with the College of Electrical Engineering and New Energy, China Three Gorges University, Yichang, China. His current research interests include distributed generation, microgrid operation and control, integrated energy system, and smart grids.

**Zhuoli Zhao** received the Ph.D. degree in electrical engineering from South China University of Technology, Guangzhou, China, in 2017. He is currently an Associate Professor with the School of Automation, Guangdong University of Technology, Guangzhou, China. His research interests include microgrid control and energy management, renewable power generation control and grid-connected operation, modeling, analysis and control of power-electronized power systems and smart grids.

**Loi Lei Lai** received the B.Sc. and Ph.D. degrees in electrical and electronic engineering from the University of Aston, Birmingham, UK, and University of London, London, UK, in 1980 and 1984, respectively. He is currently a University Distinguished Professor with Guangdong University of Technology, Guangzhou, China. He was a Pao Yue Kong Chair Professor with Zhejiang University, Hangzhou, China. His research interests include smart cities and smart grids.